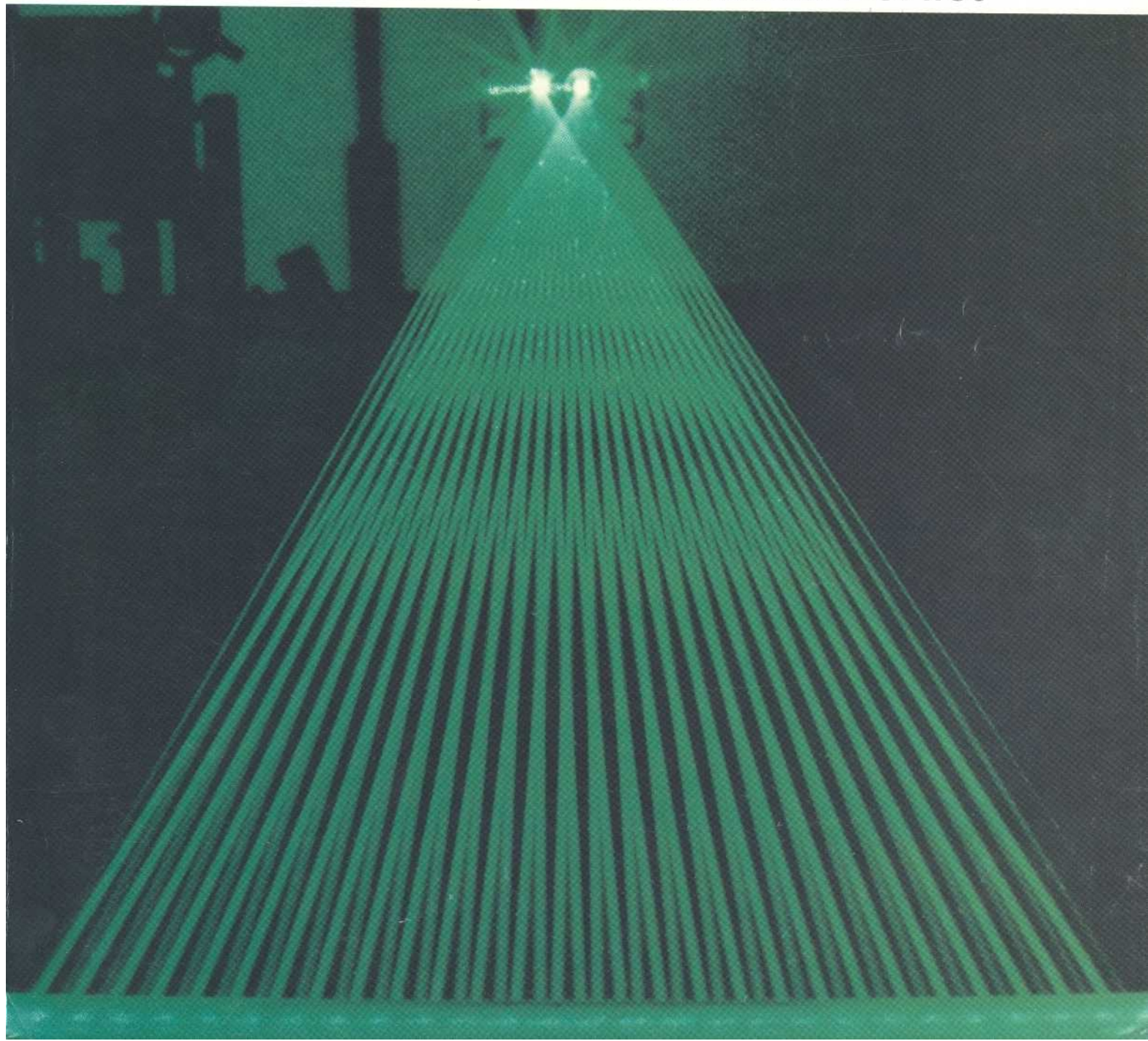


Applied Optics

20 MAY 1992

LASERS, PHOTONICS, AND ENVIRONMENTAL OPTICS



Measurements of atomic sodium in flames by asynchronous optical sampling: theory and experiment

Gregory J. Fiechtner, Galen B. King, Normand M. Laurendeau, and F. E. Lytle

Asynchronous optical sampling (ASOPS) is a pump-probe method for the measurement of species concentrations in turbulent high-pressure flames. We show that rapid measurement of species number density can be achieved in a highly quenched environment by maintaining a constant beat frequency between the mode-locking frequencies of the pump and the probe lasers. A model for the ASOPS method based on rate equation theory for three- and four-level atoms is presented. A number of improvements are made to the basic ASOPS instrument, which result in a greatly enhanced signal-to-noise ratio. Atomic sodium is aspirated into an atmospheric pressure $C_2H_4/O_2/N_2$ flame and detected with the ASOPS instrument. When excited-state lifetimes are fitted by using the ASOPS theory, a $3P_{1/2,3/2} \rightarrow 3S_{1/2}$ quenching-rate coefficient of $1.72 \times 10^9 \text{ s}^{-1}$ and a $3P_{3/2} \rightarrow 3P_{1/2}$ doublet-mixing rate coefficient of $3.66 \times 10^9 \text{ s}^{-1}$ are obtained, in excellent agreement with literature values. ASOPS signals obtained over a wide range of pump and probe beam powers validate the rate equation theory. Improvements are suggested to improve the signal-to-noise ratio, since the present results are limited to laminar flows.

Key words: Combustion, quenching, spectroscopy, atomic sodium lifetime.

I. Introduction

Optical methods of measuring species concentrations have provided new insights into the combustion process.¹ The most widely used of these techniques is laser-induced fluorescence (LIF),² because its sensitivity and low noise background permit detection of minor species. The LIF signal is related to the population being detected by

$$S_f \propto \frac{N_T}{A + Q}, \quad (1)$$

where N_T is the absolute number density of the species in question (in cubic centimeters), A is the Einstein coefficient for spontaneous emission (inverse seconds), and Q is the collisional quenching-rate coefficient (inverse seconds). This inverse dependence on Q has meant that historically, LIF studies were limited to low-pressure flames. Technological

advances, coupled with the fact that many practical combustors operate at high pressures, have resulted in a number of recent high-pressure LIF studies.³⁻⁶

A second constraint of practical flame measurements is turbulence.⁷ The quenching-rate coefficient of species p from collisions with species q is given by⁸

$$Q = \sum_q N_{T,q} \bar{v}_{pq} \sigma_{pq}, \quad (2)$$

where $N_{T,q}$ is the number density of species q , σ_{pq} is the cross section (centimeters squared), and \bar{v}_{pq} is the average relative velocity (centimeters per second), which is given by

$$\bar{v}_{pq} = \sqrt{\frac{8kT}{\pi\mu_{pq}}}, \quad (3)$$

where μ_{pq} (g) denotes the reduced mass for species p and q . Equations (2) and (3) show that turbulent fluctuations in concentration and temperature will introduce uncertainty into the LIF signal through corresponding fluctuations of Q . When measuring concentrations within the time scale of turbulence, any method that overcomes the effects of quenching must do so in a rapid manner, owing to the extremely short times in question.⁷

One approach to the quenching problem is to elimi-

F. E. Lytle is with the Department of Chemistry, Purdue University, West Lafayette, Indiana 47907. The other authors are with the Flame Diagnostics Laboratory, School of Mechanical Engineering, Purdue University, West Lafayette, Indiana 47907.

Received 4 August 1991.

0003-6935/92/152849-16\$05.00/0.

© 1992 Optical Society of America.

nate quenching as the dominant loss process. The laser-saturated fluorescence technique uses high-power lasers so that stimulated emission overwhelms quenching.² The inverse dependence of the LIF signal on quenching is thus removed by saturating the transition. However, calibration techniques must be used to take into account incomplete saturation in the wings of the laser beam spatial profile.^{9,10} In addition, saturation cannot be achieved over the entire temporal laser pulse, owing to low intensity at the leading and trailing edges. Although considerable laser power is required to saturate at high pressures, saturation of OH has been observed in high-pressure flames.^{4,6} In photoionization controlled-loss spectroscopy, a second beam induces photoionization, which effectively eliminates the sensitivity of two-photon LIF signals to quenching.¹¹ In laser-induced predissociation fluorescence, predissociation becomes the dominant loss process.¹² However, in reducing the sensitivity to quenching, each of these methods also inherently reduces the magnitude of the LIF signal.

Equation (2) suggests a different approach to quenching fluctuations. Barlow *et al.*^{13,14} detected single-shot OH fluorescence while simultaneously measuring major species concentrations and temperature by using Raman scattering. A quenching correction factor was then calculated by using known collision cross sections with OH. Barlow *et al.* found that significant errors result for rich stoichiometries if the quenching correction factor is not applied. This represents a useful method for species such as OH, which have a large available database of appropriate cross sections. For many species of interest, however, little collisional data is available. Moreover, Barlow *et al.* found it necessary to use high laser intensities to obtain a sufficient number of fluorescence photons per shot while sacrificing spatial resolution to prevent saturation.

The most direct method of correcting for quenching is to measure the fluorescence lifetime. In low-pressure flames, the method is straightforward, with a photomultiplier signal being exponentially fitted from ~90% to ~10% of the maximum signal amplitude.^{15,16} At atmospheric pressure and above, high quenching rates typically result in lifetimes of several nanoseconds or less. In this regime, picosecond lasers and ultrafast streak cameras with picosecond resolution are required. Takubo *et al.*¹⁷ have used a mode-locked laser with 30-ps pulses and a fluorescence detector to measure quenching of hydroxyl at atmospheric pressure. Because of the inadequate temporal response of the photomultiplier (~1 ns), a detailed convolution analysis was required to obtain the desired lifetimes. However, the use of a streak camera can reduce the detector response to less than a picosecond.¹⁸ Bergano *et al.*¹⁹ used a Q-switched mode-locked laser with a 10-Hz train of 5-ps pulses and a streak camera to measure an OH fluorescence lifetime of 1.8 ns in an atmospheric-pressure flame. Schwarzwald *et al.* used a home-built laser system that provided a 1-Hz train of 20-ps pulses and a

streak camera to obtain a similar value of 1.97 ns for OH,²⁰ 2.23 ns for CN,²¹ and 1.7 ns for NO.²²

Although each of the above techniques remains promising, pulsed lasers with repetition rates of roughly 10 Hz are normally required. The most rapid fluctuations are given by the Kolmogorov time.²³ Depending on flow conditions, for an atmospheric-pressure flame, these fluctuations are approximately 1 μ s.^{7,24,25} Unfortunately, the turbulence frequency spectrum that can be resolved is limited by the rate at which the laser is pulsed. Even with single-shot detection, each of the above techniques will thus not be able to resolve most of the flow-field spectral information. Clearly, a technique that uses high-repetition-rate lasers is necessary. This has led to the demonstration of an alternative lifetime-measurement technique by Alfano,²⁶ based on a subnanosecond gated photon-counting technique.²⁷ The method uses a high-repetition-rate mode-locked laser system (3.8 MHz), which permits averaged sodium decays in an atmospheric pressure flame to be obtained in less than 1 ms. However, the insufficient peak power does not permit measurement of naturally occurring flame radicals.

The inability of the fluorescence techniques to obtain reliable data in a sufficient time scale for turbulent measurements is caused by the spontaneous nature of the LIF signal. Since each molecule emits independently of all others, the statistical nature of spontaneous emission originates in the form of noise; thus any significant improvement in the temporal, spectral, or spatial resolution will result in a corresponding reduction in signal magnitude.²⁸ Stimulated absorption and stimulated emission are not subject to the same resolution constraints. Furthermore, all species absorb photons, while only a limited number of species fluoresce. Although absorption is a line-of-sight technique, spatial resolution equal to that of the LIF method can be obtained by using pump-probe spectroscopy, for which two laser beams are crossed.²⁹ Nevertheless, a comparatively small number of pump-probe combustion studies has been completed, including demonstrations by Goldsmith,³⁰ Farrow and Rahn,³¹ Goldsmith and Farrow,³² Kychakoff *et al.*,²⁹ Walters *et al.*,³³ and Omenetto *et al.*³⁴ The chief reason for the small number of experiments stems from the fact that the probe-beam signal represents a small change in intensity superimposed upon a large background, while an LIF signal represents a signal with theoretically zero background.¹ Although true in principle, many cases exist in which the difference between these two extremes is reduced. The LIF background will not always be negligible. In heterogeneous high-pressure flames, background noise from Mie scattering can severely interfere with LIF signals.³⁵ Furthermore, the pump-probe background level can be reduced quite easily with the proper choice of laser. Conventional pulsed laser systems contain significant noise that results from high-frequency mode fluctuations and are thus inappropriate for use as the probe beam. For this

reason, early experiments used single-mode cw laser systems. In addition, the low peak power of cw lasers results in a small absolute signal magnitude. The use of mode-locked lasers offers a vast improvement over cw single-mode lasers. Mode-locked lasers provide picosecond pulse widths, which result in large peak powers and high signal levels. High-frequency fluctuations present on free-running probe lasers are suppressed by the mode-locking process, which defines a fixed phase relationship between all active laser modes.^{36,37} Indeed, it has been demonstrated that for high-frequency modulation and synchronous detection, pump-probe instruments that use mode-locked probes approach the shot-noise limit,³⁸⁻⁴⁰ with a minimum detectable modulation depth that approaches 10^{-8} with 1 s of signal averaging.⁴¹

Armed with this knowledge, a number of researchers have performed pump-probe studies at high (> 3 MHz) modulation frequencies by using stimulated absorption-emission spectroscopy.⁴²⁻⁴⁵ In these conventional pump-probe instruments, the pump and probe lasers are derived from a single mode-locked source, so that both beams have the same repetition rates. Moreover, some type of mechanical or electro-optical chopping scheme is generally employed to induce an amplitude modulation on the signal, which facilitates the use of synchronous detection. The pump pulses excite the sample, and the probe pulses stimulate emission. Timing between the two beams is controlled by varying the optical path of the probe; this variation permits reconstruction of the excited-state lifetime. Thus pump-probe spectroscopy combines the advantages of stimulated absorption-emission with those of mode-locked lasers. Furthermore, this technique permits the measurement of subnanosecond decays with a simple, inexpensive photodiode detector. Despite these advantages, however, the optical delay line of the conventional pump-probe instrument causes a perplexing problem. Since the optical delay elements must be repositioned between each delay interval, excited-state lifetime measurements within the Kolmogorov microscale are impossible. This renders the instrument useless in the turbulent environment of typical combustors.

Asynchronous optical sampling (ASOPS) is a novel pump-probe method that will potentially permit the determination of number densities and quenching rates in turbulent high-pressure flames. The basic ASOPS instrument consists of two dye lasers synchronously pumped by two frequency-doubled mode-locked Nd:YAG lasers. The two lasers operate at slightly different repetition rates, which causes a relative phase walkout between the pump and the probe beams. This strategy permits the repetitive mapping of subnanosecond excitation processes in less than a millisecond. The ASOPS technique thus retains the important advantages of conventional pump-probe instruments yet eliminates the need for a cumbersome optical delay line.

Initial ASOPS studies of Rhodamine B in methanol^{46,47} and of atomic sodium in atmospheric-pressure

flames^{48,49} have previously been reported. In this paper an improved ASOPS instrument is shown to yield an excellent signal-to-noise ratio (SNR) in atmospheric flat flames doped with atomic sodium. A detailed theory is presented that demonstrates the efficacy of pump-probe lifetime measurements. When the theory is used to analyze the data, ASOPS measurements of the sodium $3P_{3/2} \rightarrow 3S_{1/2}$ and $3P_{1/2} \rightarrow 3S_{1/2}$ quenching rates and the $3P_{3/2} \rightarrow 3P_{1/2}$ doublet-mixing rate are found to agree closely with literature values. By obtaining the ASOPS signal over a wide range of pump and probe beam powers, we also determine the optimum operating parameters for the ASOPS instrument. Because of the large noise background of the mode-locked probe laser, the scan rate was 100 μ s, and averaging of many scans was necessary. Hence the present results are limited to laminar flame environments. A variety of approaches are suggested for improving the SNR, thereby potentially permitting concentrations to be obtained in turbulent flames.

II. Operating Principles

The ASOPS process is illustrated in Fig. 1(a), which shows the excited-state population produced by several pump pulses over which the temporal positions of several probe pulses have been superimposed. Each successive probe pulse is delayed in time relative to the pump pulse train by a constantly increasing duration that is determined by the beat frequency of the system. Thus each probe pulse samples the excited-state population at a slightly later time than the immediately preceding probe pulse. This is equivalent to varying the optical delay in a conventional pump-probe instrument. Figure 1(b) illustrates the change in probe intensity that occurs upon stimulated emission from the excited-state population in Fig. 1(a). The net effect of the ASOPS technique is that a small-amplitude waveform, which is directly related to the fluorescence decay of the species under study, is impressed upon the probe laser intensity. In essence, a temporal transformation of the excited-state decay is performed with the time that is scaled by the factor $f_{\text{pump}}/(f_{\text{pump}} - f_{\text{probe}})$, where f_{pump} and f_{probe} are the repetition rates of the pump and probe

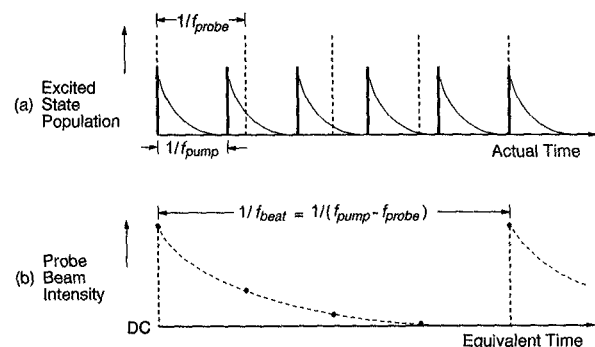


Fig. 1. ASOPS timing diagram showing (a) excited-state population and (b) probe-beam intensity upon stimulated emission. The probe pulses in (a) are indicated by vertical dashed lines.

lasers, respectively. A distinguishing factor from conventional pump-probe spectroscopy is that the sample mixes the laser repetition rates, which permits synchronous detection at the difference, or beat frequency, $f_{\text{beat}} = f_{\text{pump}} - f_{\text{probe}}$. This eliminates the need for amplitude modulation of either beam. The inverse of the pump frequency $1/f_{\text{pump}}$ gives the free temporal range of the ASOPS instrument. The total number of points N sampled during the decay is determined by $N = f_{\text{probe}}/f_{\text{beat}}$. The temporal difference between each sampled point within the decay profile is the sampling interval, determined by the difference in laser periods, or $f_{\text{beat}}/[(f_{\text{probe}})(f_{\text{pump}})]$. More importantly, the process automatically repeats at the period of the ASOPS instrument, given by $1/f_{\text{beat}}$. The ASOPS technique is thus an optical analog of the sampling oscilloscope. As such, the ASOPS instrument potentially permits a large number of averages to be obtained in a time less than that of a relevant turbulent fluctuation. Operating parameters typical of an ASOPS experiment are given in Table I.

Since the wavelengths of the pump and the probe lasers can be independently controlled, specific electronic quenching rates can be determined between the excited and the ground states. As shown in Fig. 2, the pump beam is chosen to excite atoms from level 1 to level 2. The probe connects level 2 to level 3, which can be of lower [Fig. 2(a)] or higher [Fig. 2(b)] energy than level 2. In Fig. 2(a) the probe beam undergoes gain modulation owing to stimulated emission from the excited-state population, which results in the ASOPS process of Fig. 1. If, however, level 3 is of higher energy than level 2, then the probe will undergo loss modulation because of the absorption by excited-state molecules [Fig. 2(b)]. The resulting ASOPS process is demonstrated in Fig. 3. The chief difference is that the ac signal obtained by using excited-state absorption will be of negative amplitude compared to the signal obtained by using excited-state emission. It is also possible to tune both the pump and the probe beams to the same transition. In this case, modulation of the probe will take place as a result of both excited-state emission and ground-state absorption.⁴⁹

III. Fundamental Theory

The basic theory for ASOPS can be explicated based on the simple three-level system shown in Fig. 2. Again, the pump beam is chosen to excite atoms from

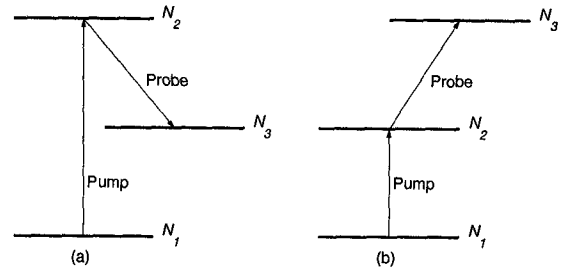


Fig. 2. Three-level pump-probe model. The probe beam is modulated as a result of (a) stimulated emission or (b) excited-state absorption.

level 1 to level 2. The wavelength of the probe beam is then chosen to stimulate either [Fig. 2(a)] absorption to a nearby upper level or [Fig. 2(b)] emission to a nearby lower level, both denoted by level 3. The following theory will now be developed by considering in turn the separate processes of laser pumping, excited-state decay, and laser probing. Eventually, two equations will be obtained that contain two unknowns, the excited-state lifetime and the ground-state number density. Using Boltzmann statistics, we can then obtain the total number density from the ground-state number density.

A. Three-Level Model

Consider first the interaction of the pump laser with the sample. When a pump-beam pulse passes through the sample, excitation is governed by the rate equation

$$\frac{dN_1}{dt} = -N_1 W_{12}, \quad (4)$$

where N_1 is the ground-state number density and W_{12} is the stimulated absorption rate coefficient between levels 1 and 2. Assuming a constant laser power over the temporal width of the laser pulse, we integrate to get

$$N_1 = N_1^0 \exp(-W_{12} \Delta t_{12}), \quad (5)$$

where Δt_{12} is the temporal width of the individual pump pulses and N_1^0 is the number density of level 1 in the absence of laser radiation. For a typically weak

Table I. Typical Operating Parameters for ASOPS

Pump repetition rate (f_{pump})	81.5934762 MHz
Probe repetition rate (f_{probe})	81.5836420 MHz
Beat frequency ($f_{\text{pump}} - f_{\text{probe}}$)	9.8342 kHz
Free temporal range ($1/f_{\text{pump}}$)	12.256 ns
Samples per decay ($f_{\text{probe}}/f_{\text{beat}}$)	8296
Sampling interval ($f_{\text{beat}}/f_{\text{probe}}f_{\text{pump}}$)	1.4773 ps
Pump power	20 mW
Probe power	5 mW
Pulse width	20 ps
Bandwidth	0.04 nm

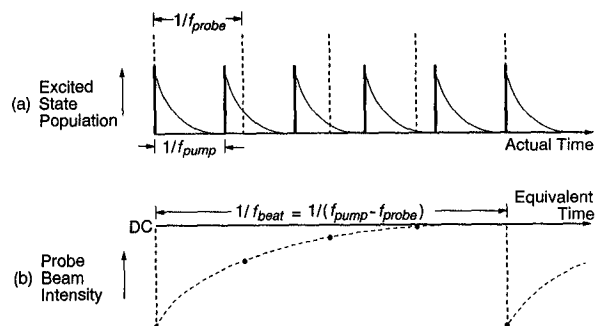


Fig. 3. ASOPS timing diagram corresponding to excited-state absorption.

laser beam, expansion of the exponential in Eq. (5) yields

$$N_1 = N_1^0(1 - W_{12}\Delta t_{12}). \quad (6)$$

Since the pump beam connects only levels 1 and 2, any loss in the population of level 1 must appear in level 2. Thus the number density in level 2 immediately after a pump pulse must be

$$N_2^0 = N_1^0 W_{12} \Delta t_{12}, \quad (7)$$

as can be seen from Eq. (6). This development is analogous to that for the time-resolved LIF technique, in which excitation and detection of fluorescence is carried out in a period much less than that of quenching.⁵⁰⁻⁵²

In the absence of laser radiation, i.e., between laser pulses, the temporal behavior of the excited-state population is described by the rate equation

$$\frac{dN_2}{dt} = -(A_{21} + Q_{21})N_2 = -\frac{N_2}{\tau}, \quad (8)$$

where A_{21} is the Einstein coefficient for spontaneous emission from level 2 to level 1, Q_{21} is the quenching-rate coefficient from level 2 to level 1, and τ is the lifetime of the excited state. Since $\tau \gg \Delta t_{12}$, integration of Eq. (8) gives

$$N_2^* = N_2^0 \exp\left(-\frac{t}{\tau}\right), \quad (9)$$

and substitution of Eq. (7) into Eq. (9) yields

$$N_2^* = N_1^0 W_{12} \Delta t_{12} \exp\left(-\frac{t}{\tau}\right). \quad (10)$$

As for the pump pulse, the excitation dynamics induced by the probe-beam pulse is described by the rate expression

$$\frac{dN_2}{dt} = -N_2 W_{23}, \quad (11)$$

where W_{23} is the stimulated rate for either emission [Fig. 2(a)] or excited-state absorption [Fig. 2(b)] between levels 2 and 3. Integration of Eq. (11) gives

$$N_2 = N_2^* \exp(-W_{23}\Delta t_{23}), \quad (12)$$

where Δt_{23} is the temporal width of the individual probe pulses ($\Delta t_{23} \ll \tau$). Again, expanding the exponential term of Eq. (12) gives

$$N_2 = N_2^*(1 - W_{23}\Delta t_{23}). \quad (13)$$

The probe beam connects levels 2 and 3; thus any population that is stimulated from level 2 must arrive in level 3, so that

$$N_3 = N_2^* W_{23} \Delta t_{23}. \quad (14)$$

Those atoms arriving in level 3 must necessarily modulate the probe beam. The time-dependent ASOPS signal is hence given by

$$S(t) = \eta_o \eta_e N_3 V_c, \quad (15)$$

where η_o is the optical efficiency, η_e is the efficiency of the detection electronics (V/photon), and V_c is the collection volume (cm^3). Substituting from Eqs. (10) and (14) and defining the overall detection efficiency $\eta = \eta_o \eta_e$, we obtain

$$S(t) = \eta W_{12} \Delta t_{12} W_{23} \Delta t_{23} V_c N_1^0 \exp\left(-\frac{t}{\tau}\right). \quad (16)$$

This temporal signal is obtained by using a digitizing oscilloscope in the present experiments. Integration of the time-dependent ASOPS signal represents the signal-averaging process that is employed in most diagnostic experiments, e.g., the use of a boxcar averager. Integration of Eq. (16) yields the time-averaged ASOPS signal

$$S_A = \int_0^\infty S(t) dt = \eta W_{12} \Delta t_{12} W_{23} \Delta t_{23} V_c \tau N_1^0. \quad (17)$$

Equation (17) indicates that after determining the calibration parameter $C = \eta W_{12} \Delta t_{12} W_{23} \Delta t_{23} V_c$, we have only the unknowns τ and N_1^0 . The collisional lifetime can be obtained from the temporal decay represented by Eq. (16). Since $N_1^0 = S_A / C\tau$, the absolute total number density can be determined by simultaneously correcting for the effects of the quenching environment.⁵⁰⁻⁵²

B. Multilevel Atomic Model

The measurement of naturally occurring flame radicals such as OH is of crucial importance in combustion. However, the absorption resonances for OH fall in the ultraviolet region of the spectrum. This produces two difficulties with respect to the ASOPS instrument: (1) the visible output of the synchronously pumped dye lasers must be frequency doubled, which greatly reduces the power available for experiments; and (2) frequency doubling increases the baseband noise on the pump and the probe beams by approximately two orders of magnitude, and it increases the bandwidth by approximately a factor of two.⁵³ For these reasons the ASOPS measurements reported here have been done on atomic sodium. Although sodium is present in marine-based fuels⁵⁴ and has been the subject of kinetic studies in hydrocarbon flames,⁵⁵ it is usually seeded into flames and subsequently detected for the following reasons: (1) sodium is comparatively easy to atomize into flames, (2) the absorption cross section for sodium is three orders of magnitude larger than that of most molecular species, (3) the well-known sodium *D* lines are located near the peak of the gain curve of the most efficient laser dyes, and (4) the resulting yellow laser beams are easily aligned by visual detection.

Because of spectroscopic doublets, models for so-

dium and the other alkalis require an additional energy level. The sodium doublet in particular results in the D_1 and D_2 lines at 589.6 and 589.0 nm, respectively.⁵⁶ This means that level 2 of the three-level model of Fig. 2 must be split into two levels, as shown in Fig. 4. Level 1 is again the ground state ($3S_{1/2}$), and levels 2 and 3 are reserved for the doublet states ($3P_{1/2}$ and $3P_{3/2}$, respectively). Level 4 is a level of higher energy ($4D_{5/2,3/2}$ or $5S_{1/2}$) that can be connected to either level 2 or 3 by the probe laser. Although several researchers have given derivations for similar models,⁵⁷ the following analysis is now presented specific to the ASOPS method. Here, R_{ij} and R_{ji} represent the rate coefficients of upward and downward population exchange, respectively. The upward-rate coefficients can be expressed as

$$R_{ij} = W_{ij} + Q_{ij}, \quad (18)$$

and the downward-rate coefficients become

$$R_{ji} = W_{ji} + Q_{ji} + A_{ji}. \quad (19)$$

The rate equations for levels 2 and 3 after the pump pulse has traversed the sample are then given by

$$\frac{dN_2}{dt} = N_2' = R_{12}N_1 - (R_{21} + R_{23})N_2 + R_{32}N_3, \quad (20)$$

$$\frac{dN_3}{dt} = N_3' = R_{13}N_1 + R_{23}N_2 - (R_{31} + R_{32})N_3. \quad (21)$$

The ground-state number density can be eliminated from the rate equation, since

$$N_1 = N_T - (N_2 + N_3), \quad (22)$$

where N_T is the total number density. Thus

$$N_2' = -(R_{12} + R_{21} + R_{23})N_2 + (R_{32} - R_{12})N_3 + R_{12}N_T, \quad (23)$$

$$N_3' = (R_{23} - R_{13})N_2 - (R_{13} + R_{31} + R_{32})N_3 + R_{13}N_T. \quad (24)$$

These relations can now be solved for excited-state relaxation after pump-beam excitation, for which $W_{ij} = W_{ji} = 0$. The quenching-rate coefficient ratios

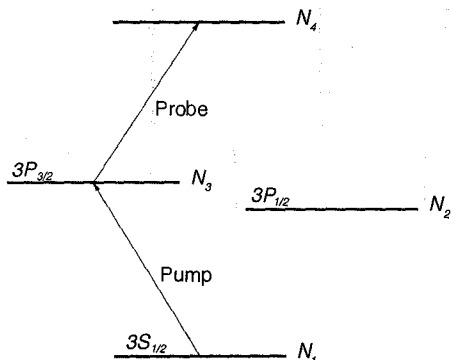


Fig. 4. Four-level sodium model. Levels 1, 2, and 3 correspond to the $3S_{1/2}$, $3P_{1/2}$, and $3P_{3/2}$ states, respectively. Level 4 represents either the $4D_{5/2,3/2}$ or $5S_{1/2}$ states in the present experiments.

are given by⁵⁸

$$\frac{Q_{21}}{Q_{12}} = \frac{g_1}{g_2} \exp[-(E_1 - E_2)/kT], \quad (25)$$

$$\frac{Q_{31}}{Q_{13}} = \frac{g_1}{g_3} \exp[-(E_1 - E_3)/kT], \quad (26)$$

which for atomic sodium at 1000 K become 4×10^{10} and 2×10^{10} , respectively. Hence we may assume that $Q_{12} = Q_{13} = 0$. This also means that little of the total population will initially be in the excited state, so that $N_1^0 = N_T$. In addition, since only 0.6 nm separates the D_1 and D_2 lines, it will be assumed that $Q_{21} = Q_{31} = Q$. Furthermore, $Q \sim 2 \times 10^9 \text{ s}^{-1}$ in an atmospheric-pressure hydrocarbon flame,⁵⁹⁻⁶¹ and $A = 6.15 \times 10^7 \text{ s}^{-1}$ (Ref. 62), so that A_{ji} can be ignored. Under these assumptions, the time-dependent number densities of excited sodium become

$$N_2(t) = \frac{Q_{32}}{Q_{23} + Q_{32}} (N_2^0 + N_3^0) \exp(-Qt) + \left(\frac{Q_{23}}{Q_{32}} N_2^0 - N_3^0 \right) \exp[-(Q + Q_{23} + Q_{32})t], \quad (27)$$

$$N_3(t) = \frac{Q_{23}}{Q_{23} + Q_{32}} (N_3^0 + N_2^0) \exp(-Qt) + \left(\frac{Q_{32}}{Q_{23}} N_3^0 - N_2^0 \right) \exp[-(Q + Q_{23} + Q_{32})t]. \quad (28)$$

Note that N_2^0 is given by Eq. (7) and that N_3^0 is analogously defined. These represent the number densities in levels 2 or 3 immediately after the pump pulse. In the present experiments, either N_2^0 or N_3^0 will be zero, since only a single transition is pumped. For $N_3^0 = 0$, these relationships are identical to those presented by Takubo *et al.*⁵⁹ A further assumption is obtained by relating levels 2 and 3 by using the principle of detailed balancing,⁵⁸

$$\frac{Q_{23}}{Q_{32}} = \frac{g_3}{g_2} \exp[-(E_3 - E_2)/kT], \quad (29)$$

which equals 1.95 at 1000 K. Thus little error is incurred in assuming that $Q_{23} = 2Q_{32}$. The number densities of the excited doublets are then

$$N_2(t) = \frac{1}{3} (N_2^0 + N_3^0) \exp(-Qt) + (2N_2^0 - N_3^0) \exp[-(Q + 3Q_{32})t], \quad (30)$$

$$N_3(t) = \frac{2}{3} (N_3^0 + N_2^0) \exp(-Qt) + (0.5N_3^0 - N_2^0) \exp[-(Q + 3Q_{32})t]. \quad (31)$$

The influence of the doublet within the four-level model on the ASOPS signal must now be examined. Suppose that the pump laser has been tuned to excite atoms to level 3 ($3P_{3/2}$), while the probe is tuned between levels 3 and 4. Then $N_3(t)$ will be given by Eq.

(31) with $N_2^0 = 0$ and $N_3^0 = N_T W_{13} \Delta t_{13}$. In analogy with Eq. (9) for the three-level model, $N_3^* = N_3(t)$. The probe excitation dynamics will also be similar, with $N_4(t) = N_3^* W_{34} \Delta t_{34}$, where W_{34} is the stimulated-rate coefficient between levels 3 and 4 and Δt_{34} is the pulse width of the probe beam. Since any atoms reaching level 4 will modulate the probe beam, the time-dependent ASOPS signal as seen on an oscilloscope will be given by $S(t) = \eta N_4(t) V_c$, so that

$$S(t) = \eta W_{13} \Delta t_{13} W_{34} \Delta t_{34} V_c N_T \left\{ \exp(-Qt) + \frac{1}{2} \exp[-(Q + 3Q_{32})t] \right\}, \quad (32)$$

where the factor of 2/3 has been absorbed into η . The time-averaged ASOPS signal will again be obtained by integration of Eq. (32), which yields

$$S_A = \eta W_{13} \Delta t_{13} W_{34} \Delta t_{34} V_c N_T \left(\tau_1 + \frac{1}{2} \tau_2 \right), \quad (33)$$

where $\tau_1 = \tau$ and $\tau_2 = (Q + 3Q_{32})^{-1}$.

Pumping of level 3 will also result in atoms reaching level 2 by the use of the doublet mixing rate Q_{32} . Thus if the probe connects levels 2 and 4, then from Eq. (30) the signal becomes

$$S(t) = \eta W_{13} \Delta t_{13} W_{24} \Delta t_{24} V_c N_T [\exp(-Qt) - \exp[-(Q + 3Q_{32})t]], \quad (34)$$

and the corresponding time-averaged signal becomes

$$S_A = \eta W_{13} \Delta t_{13} W_{24} \Delta t_{24} V_c N_T (\tau_1 - \tau_2). \quad (35)$$

At $t = 0$, $S(t)$ vanishes; hence the temporal ASOPS signal rise time and decay can be fitted by using Eq. (34). Note that unlike the three-level model, the four-level case will result in two equations with three unknowns. As will be seen below, this complicates the interpretation of data obtained for atomic sodium. Takubo *et al.*^{59,63} alleviated this difficulty by monitoring broadband fluorescence from both D lines to obtain Q , after which narrowband detection yielded Q_{32} . Because of the bandwidth of the present mode-locked laser system, such experiments were not performed with the ASOPS instrument.

For detection of molecules, there are many more relaxation pathways than for the present case of atomic sodium. This could greatly complicate the analysis of ASOPS signals. We hope to eventually detect the hydroxyl radical. An advantage of OH detection is that a large amount of collisional data is available from which these complicated effects can be modeled. Using a suitable numerical model,⁴ one could delineate the complications that may arise when detecting OH. This is a subject for further study.

IV. Experimental Apparatus

Since the ASOPS technique requires that the pump and probe lasers operate at slightly different repeti-

tion rates, two independent mode-locked laser systems are needed. Both the pump and probe beams are derived from Spectra-Physics model 375B dye lasers, which are synchronously pumped by frequency-doubled mode-locked Spectra-Physics series 3000 Nd:YAG lasers. Rhodamine 6G is used as the laser dye. Average powers in excess of 300 mW are obtained from the dye lasers by using 1.0–1.2 W of pumping power. The mode-locking frequencies are generated by two Programmed Test Sources model 160 frequency synthesizers operated in a master–slave (i.e., phase-locked) configuration. The resulting laser output consists of an ~ 82 MHz pulse train from each laser. The Programmed Test Sources synthesizers are accurate to 0.1 Hz; hence the laser repetition rates are very stable.

In early ASOPS studies,^{48,49} wavelength tuning was afforded by three-plate birefringent filters in the dye-laser cavities, so that both beams consisted of ~ 6 – 7 -ps pulses. If the Fourier-transform limit is assumed to hold, the spectral bandwidth for both beams was ~ 0.14 nm. Because of the short temporal pulse width, long-term laser stability was poor. In the present experiments, a Spectra-Physics 0411-6502 ultrafine étalon is added to each dye-laser cavity. This improves the long-term stability of the dye lasers from minutes to hours. Pulse widths of approximately 10 ps can now be obtained with only a minor loss in output power. In previous research,⁴⁹ the experiment was performed with the lasers adjusted to produce the smallest second-harmonic generation autocorrelation pulse widths. In the present experiments, slightly shortening the cavity increases the laser pulse width to 20 ps, which reduces the bandwidth to 0.04 nm (if the Fourier-transform limit is assumed to hold). The linewidths for atomic sodium owing to Doppler broadening and collision broadening with N_2 at 1 atm and flame temperatures can be estimated at ~ 0.001 and ~ 0.03 nm, respectively.⁶⁴ Thus the shortened cavity should yield a larger signal owing to better coupling. Furthermore, dye-laser noise also decreases near this cavity length. The noise reduction takes place over a wide frequency range, as shown in Fig. 5, which contains two noise spectra as measured on a Hewlett-Packard 8553L/8552B/141T rf spectrum analyzer. In the top plot [Fig. 5(a)] the noise present on a minimum autocorrelation pulse-width beam is shown. In the lower plot [Fig. 5(b)] the noise present on the probe beam when the cavity length has been reduced by 28 μm is shown. It is not known why dye-laser noise drops so significantly at the shorter cavity position.

A block diagram of the ASOPS instrument is shown in Fig. 6. To obtain the trigger signal, a synchronous voltage output from each synthesizer is first amplified with a rf power amplifier (Electronic Navigation Industries 503L) and then electronically mixed by a double-balanced mixer (Anzac MDC-161). Note that the output frequency of each synthesizer is half that of the optical repetition rate; Anzac DI-4 electronic frequency doublers between the power

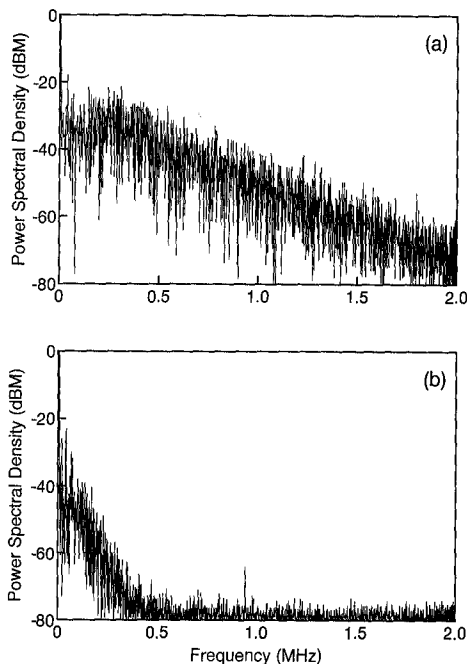


Fig. 5. Comparison of dye-laser noise for two different cavity lengths obtained by using a Hewlett-Packard 8553L/8552B/141T rf spectrum analyzer. The top plot (a) contains the noise at the minimum autocorrelation pulse-width cavity length. The lower plot (b) contains the noise when the cavity has been shortened by 28 μm .

amplifiers and the double-balanced mixer generate a trigger signal at the beat frequency of the system. The mixer output passes through a 4LM5-3-CD Texscan 5-MHz low-pass filter to remove any high frequencies leaking through the mixer. The output of the filter then enters a digital delay generator (Berkeley Nucleonics Corporation 7095), which produces a stable 0–5-V trigger pulse of variable width. Unlike the optical triggering scheme previously employed,^{46–49}

this new electronic scheme offers much less temporal jitter in the trigger pulse and thus offers an improved SNR.

The pump and the probe beams are first passed through calibrated neutral density filters that provide a convenient means of varying the power in either beam. The two beams then pass through a single focusing lens ($f = 100 \text{ mm}$) and cross at an included angle of $\sim 5^\circ$ in the flame, each with a beam waist of approximately 46 μm , which results in an effective Beer's law path length³⁶ of $\sim 530 \mu\text{m}$. Despite this small beam waist, diffusion of sodium atoms out of the pump region is not an important consideration.⁶¹ The probe beam is recollimated by a matching lens. In previous experiments, the probe beam was then monitored by a photodiode (EG&G SGD-100A), the output of which was filtered with a 4LM5-3-CD Texscan 5-MHz low-pass filter to remove the 82-MHz pulses and any other high-frequency noise. It has since been found that a great deal of noise on the probe beam is coherent, with structure at or below 100 kHz.⁶⁵ Coherent-noise structure cannot be eliminated effectively by signal averaging. Thus the present experiments use the differential detector of Fig. 7, which includes two EG&G FND-100Q photodiodes. Half of the probe beam is split off before the flame and is detected by one of the photodiodes. The remainder of the probe passes through the flame and is detected by the second photodiode. The intensity of light at the first photodiode is adjusted with a polarization rotator–polarization beam splitter combination until it equals the intensity of light at the second photodiode. Since the ASOPS signal is detected by the second photodiode exclusively, it will be unaffected by the subtraction process. The signal from each photodiode reaches an Analog Devices AD 521 instrumentation amplifier. Efficient subtraction takes place as a result of the high common-mode rejection ratio (CMRR) of the amplifier (CMRR $\cong 70 \text{ dB}$ minimum).

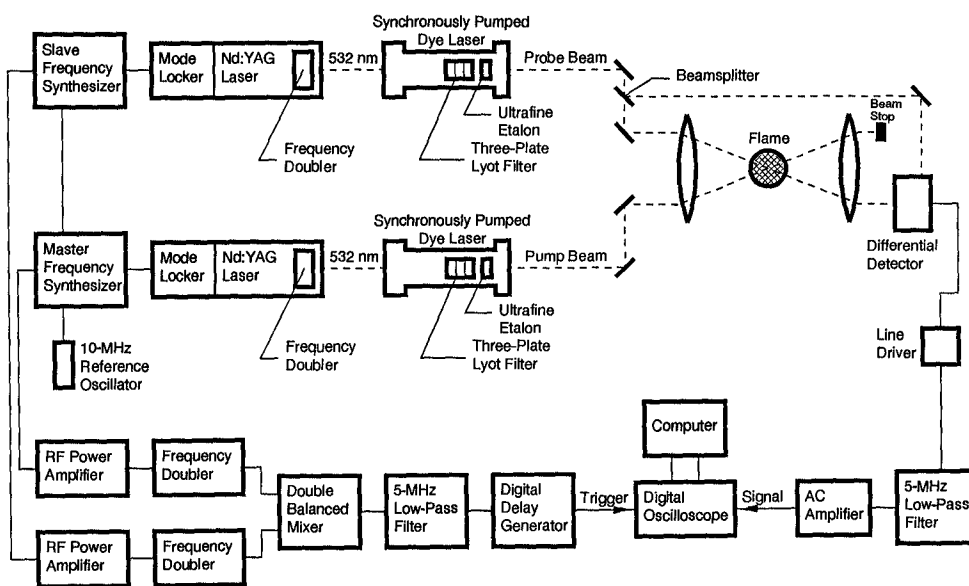


Fig. 6. Diagram of the ASOPS instrument.

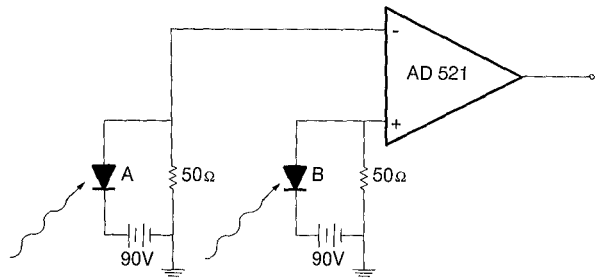


Fig. 7. Differential detector. Both photodiodes are EG&G FND-100Q, which have a rise time of < 1 ns. Before the flame, half of the probe beam is split off and reaches photodiode A. The postflame half of the probe beam reaches photodiode B. Since the ASOPS signal is contained only in the half of the probe that reaches photodiode B and the noise is present on both halves of the probe, only the noise is attenuated.

Figure 8 contains an ASOPS signal that was measured on a Hewlett-Packard Model 3580A spectrum analyzer, which has an optimum operating range of 5 Hz to 50 kHz. The displayed signal corresponds to a 200-mW pump beam at 589.0 nm and a 5-mW probe beam at 568.8 nm, with ac amplification of $100\times$. The top trace of the figure resulted when the preflame portion of the beam was blocked, so that the second portion was exclusively monitored. The bottom trace was obtained for the case in which both portions of the probe have equal intensity, i.e., full subtraction takes place. The structures occurring every 9.9 kHz are harmonics of the ASOPS signal, since at the time of the measurement the beat frequency was 9.9 kHz. As expected, the ASOPS harmonics pass unaffected by the subtraction process. However, the noise is attenuated by at least an order of magnitude. More importantly, coherent structure is reduced with equal or higher efficiency. The form of the ASOPS signal in

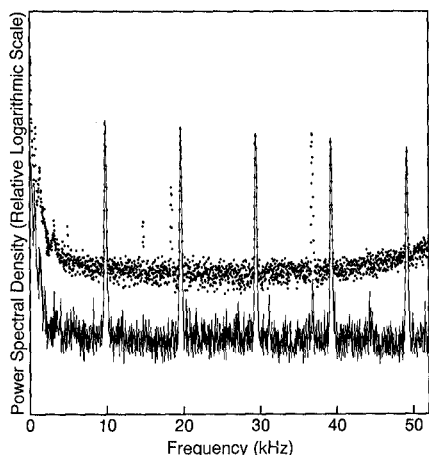


Fig. 8. Demonstration of differential detector. The top curve (points) corresponds to an ASOPS signal detected with a single photodiode, and the bottom curve (solid) corresponds to the same ASOPS signal during voltage subtraction. The spikes that occur every 9.9 kHz are harmonics of the ASOPS signal, since the beat frequency happened to be 9.9 kHz on that occasion. The ASOPS harmonics are of equal magnitude for both curves, since only the background noise is attenuated with the circuit.

Eq. (35) indicates that division by the reference intensity is a better way to remove probe beam fluctuations. However, we have found analog dividers to be comparatively noisy. In addition, the division bandwidth is inadequate for the beat frequencies necessary for turbulent concentration measurements.

The AD 521 instrumentation amplifier cannot drive 50- Ω inputs, and thus an Analog Device HOS-050 video operational amplifier is implemented as a line driver. The output from the video amplifier then passes through a Texscan 4LM5-3-CD 5-MHz low-pass filter, and the output from the filter is amplified by a C-COR 4375-A wideband ac amplifier (see Fig. 6). The AD 521 and AD HOS-050 have gain set at unity to ensure that the C-COR AC amplifier is not saturated by the output voltage. For the temporal studies, the output from the ac amplifier is directed to a digitizing oscilloscope (Hewlett-Packard 54100A), triggered at the beat frequency of the system.

In the power studies presented below, the lasers are instead directed through the optical setup shown in Fig. 9. The pump beam is passed through a Newport 935-5 attenuator to vary pump power in the flame. To vary probe power, the probe beam is directed through a polarization rotator-polarization beam splitter combination. For each attenuating element, hysteresis effects are carefully avoided. The polarization rotator-polarization beam splitter combination provides a limited range of attenuation, so that it is necessary to place calibrated neutral density filters in the path of the probe beam. Because of the need to maintain a constant sample volume in the flame, any beam wander caused by attenuating elements must be minimized. For this reason, all components are placed within 30 cm of the 100-mm focusing lens. To monitor the extent of beam wander, glass plates are placed in the path of each beam after the flame, splitting off tiny portions to targets 3 m away. The attenuator and polarization rotator cause negligible beam wander when carefully aligned and placed near the flame. However, the neutral density filters cause beam steering that cannot be ignored. To correct for this effect, the probe beam is directed through an aperture prior to the flame. When the polarization rotator-

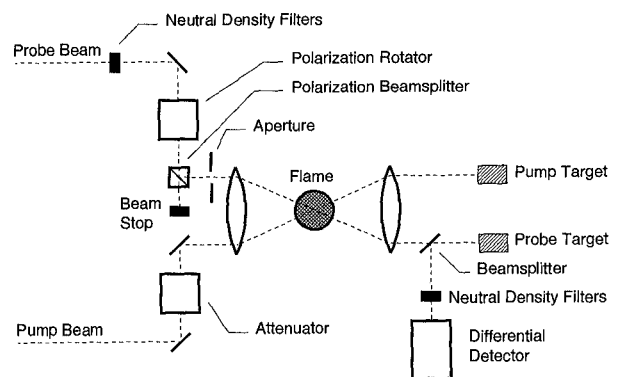


Fig. 9. Diagram of the optical setup used in the pump-probe power studies.

beam splitter combination reaches the extent of its attenuation, the ASOPS signal is recorded. A neutral density filter is then inserted into the probe path, after which the beam is centered in the aperture and the postflame target. The polarization rotator is then adjusted so that the probe power matches that of the previously recorded signal, and the resulting ASOPS signal is recorded. Any changes in signal level are accounted for during reduction of the raw data. Using this procedure, we see that corrections for changes in signal level caused by beam walking remain below 5%.

Although the detector of Fig. 7 is again used, one of the photodiodes is blocked, owing to the amount of fine tuning required to optimize noise subtraction. This prevents the experiment from taking a prohibitive amount of time to complete and removes uncertainty from the experimental results. The ac amplifier output is then directed to a Stanford Research Systems SR510 lock-in amplifier, which is triggered at the beat frequency. Both pre- and posttime constants are set to 1 s on the lock-in amplifier, and data is collected for 10 s at a sampling rate of 10 Hz. Each resulting data point represents an average over the 10-s sampling window.

The slot-burner system of our previous experiments^{48,49} proved to be extremely unreliable. The horizontal profile was often highly nonuniform and heavily dependent on the flow rate of gases. Similar slot-burner behavior was reported by Goldsmith³⁰ and by Goldsmith and Farrow.³² As noted by Alkemade *et al.*,⁶⁶ flames produced on slot burners are "less stable, homogeneous, and 'quiet' than those produced on Meker or porous-plate burners." It is thus not surprising that the slot burner used in the initial ASOPS experiments was prone to periodic surges in sodium concentration, with flame conditions changing significantly for periods of the order of minutes. Flashback through the boundary layer of the slot burner was also a frequent occurrence.

Since the ASOPS experiments presented below lasted for several hours, the slot burner was replaced by a flat-flame burner system. The same nebulization chamber was used. A 500- $\mu\text{g}/\text{ml}$ NaCl solution is directed to the nebulization chamber by a multistaltic pump at 1 ml/min, after which the mist droplets are carried to the burner by means of the combined O_2/N_2 flow. A mixing chamber packed with glass beads ensures thorough mixing of the fuel (C_2H_4) with the oxidant-diluent flow. The oxygen, nitrogen, and ethylene flow rates are 1.7, 6.0, and 0.453 L/min, respectively. The flame (equivalence ratio of 0.8) is supported by a water-cooled 30.2-mm-diameter Hastelloy-X plug. Atomization efficiency typically ranges from 1% to 15% for indirect atomization,⁶⁶ and the atomization efficiency is observed to be extremely poor for the present system, since the waste NaCl solution flow rate from the nebulizer was $\sim 95\%$ of the flow rate of the NaCl solution into the nebulizer. Assuming a conservative atomization efficiency of 5%, we estimate a sodium concentration of ~ 1 part in 10^6 in the flame.

V. Results and Discussion

The ASOPS signal of Fig. 10 is obtained by using the experimental parameters of Table I, with the pump and probe beams crossing 1 mm above the burner surface. The pump beam is tuned to the $3S_{1/2} \rightarrow 3P_{3/2}$ transition (589.0 nm) and the probe beam is tuned to the $3P_{1/2} \rightarrow 5S_{1/2}$ transition (615.4 nm). Pump and probe beam powers are 20 and 5 mW, respectively, as measured by two Laser Precision Corporation Rk-5100 pyroelectric radiometers. A peak SNR of 39:1 results after 256 averages on the digitizing oscilloscope.

ASOPS decays can be fitted to obtain the quenching-rate coefficient Q and the doublet-mixing rate coefficient Q_{32} . The above ASOPS decay is governed by Eq. (34). Obtaining a good fit to the data will thus be complicated by the fact that there are two unknowns: Q and Q_{32} . However, a large amount of data has been published relating these two parameters. The ratio Q/Q_{32} was found to be 0.47 by Takubo *et al.*⁵⁹ and 0.475 by Zizak.⁶⁷ The data of Fig. 10 are fitted with a least-squares analysis in terms of Q with the assumption $Q/Q_{32} = 0.47$. The fit corresponds to $Q = 1.72 \times 10^9 \text{ s}^{-1}$, with a relative error of 0.04%. This relative error is not meant to imply that quenching remains constant within the bound over long periods of time throughout the flame. In fact, the quenching-rate coefficient was found to vary between 1.3×10^9 and $2.0 \times 10^9 \text{ s}^{-1}$ for different experimental runs. This variation can be attributed to fluctuations in flame temperature and composition, to position in the flame, and to the fluctuating amount of water reaching the flame from the nebulizer and its resulting effects on combustion. Nevertheless, the spread of values in Q in the present experiments compares

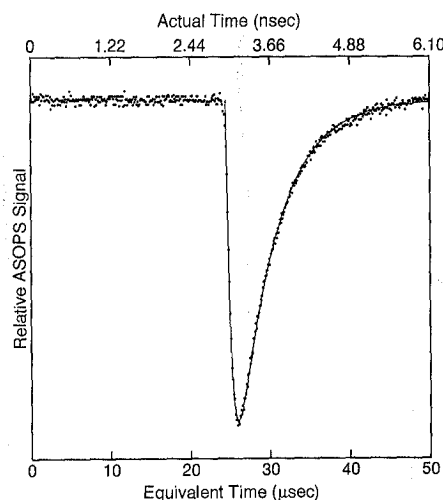


Fig. 10. ASOPS signal obtained with the pump beam (20 mW) tuned to the $3S_{1/2} \rightarrow 3P_{3/2}$ transition and the probe beam (5 mW) tuned to the $3P_{1/2} \rightarrow 5S_{1/2}$ transition. The pump and probe beams are crossed 1 mm above the burner surface, and a peak SNR of 39:1 results after 256 averages on the digitizing oscilloscope. A curve fitted under the assumption $Q/Q_{32} = 0.47$ in Eq. (34) is plotted over the data. The fit corresponds to $1/Q = 581 \text{ ps}$, with 0.04% relative error.

favorably with literature values of $Q = 1.4 \times 10^9 \text{ s}^{-1}$ reported by Takubo *et al.*⁵⁹ in a propane-air flame and by Russo and Hieftje⁶⁰ in an acetylene-air flame, $Q = 1.8 \times 10^9 \text{ s}^{-1}$ reported by Alfano in a methane-oxygen-nitrogen flame,²⁶ and $Q = 2.1 \times 10^9 \text{ s}^{-1}$ reported by Russo and Hieftje in a natural gas-air flame.⁶⁰ Similar values for the quenching-rate coefficient are obtained in the present investigation when exciting a variety of different transitions.⁶⁵

We now present a detailed study of the effects of pump and probe powers on the ASOPS signal. This study was undertaken for several reasons. First, because the laser pulse width is small compared to the excited-state lifetime, there is a question of the validity of the rate equations.^{2,68} For detection of atomic lithium in an atmospheric-pressure flame with picosecond pulses, Langley *et al.*⁴²⁻⁴⁴ have shown that the rate equations provide an excellent model for pump-probe absorption data, provided that saturation is avoided. Second, the validity of the theory required evaluation. Although Elzinga *et al.*⁴⁷ demonstrated the linearity of the ASOPS signal with both pump and probe power in a dye solution, no such results have yet been obtained in a flame environment. Finally, it was desired to locate the optimum pump and probe powers to maximize the SNR.

For infinite laser irradiance, the two-level rate equations reduce to²

$$N_2 = \frac{N_T g_2}{g_1 + g_2} \quad (36)$$

Eqs. (7) and (36) can be solved simultaneously to obtain an estimate of the saturated stimulated absorption-rate coefficient⁵⁷

$$W_{12}^{\text{SAT}} = \frac{g_2}{(g_1 + g_2)\Delta t_{1/2}} \quad (37)$$

For a laser bandwidth $\Delta\nu_{1/2}^L$ that is much larger than the medium linewidth $\Delta\nu_{1/2}$ the absorption-rate coefficient can be expressed⁶⁹

$$W_{12} = \frac{2B_{12}I}{\pi c \Delta\nu_{1/2}^L} \quad (38)$$

where I is the laser irradiance (in watts per squared centimeter). Assuming transform-limited 10-ps pulses ($\Delta\nu_{1/2}^L = 5 \times 10^{10} \text{ s}^{-1}$) and assuming a top-hat temporal profile, we predict a saturation power of $\sim 2 \text{ mW}$ for the sodium $3S_{1/2} \rightarrow 3P_{3/2}$ transition.

For these experiments, the pump is tuned to the $3S_{1/2} \rightarrow 3P_{3/2}$ transition (589.0 nm), while the probe is tuned to the $3P_{3/2} \rightarrow 4D_{5/2,3/2}$ transition (568.8 nm). The maximum available pump and probe powers in the flame are 240 and 300 mW, respectively. The pump power is varied from 3 to 240 mW, while the probe power is varied from 25 μW to 50 mW. Five different pump and probe powers are selected within these ranges. If required, neutral density filters are placed immediately before the detector to hold the probe power striking the photodiode below 10 mW,

thus keeping the photodetector within its linear range.

The ASOPS signal is plotted versus pump power for each probe power on a log-log scale in Fig. 11. As shown, the linear range extends to 30 mW in each case. In the present experiments, saturation generally becomes significant between 30 and 40 mW. This differs from the saturation curves obtained for sodium in a slot-burner flame,⁴⁹ when saturation was observed to begin between 50 and 60 mW. A probable cause is the difference between the collinear-beam and crossed-beam geometries. The saturation power for both experiments is significantly larger than that predicted above. The larger experimentally observed saturation power may have resulted from a combination of several factors. First, the calculations assume a top-hat laser profile, and they ignore the transverse distribution of laser irradiance across the laser profile. In fact, saturation will not be observed in the temporal and transverse wings of the laser. This effect is commonly observed when using the laser-saturated fluorescence technique.^{4,9,10,69} Second, in the present experiments, the pump beam will be absorbed by sodium atoms before reaching the interaction volume, since the beams were crossed near the center of the burner. Mallawaarachchi *et al.*⁷⁰ corrected their results for this effect, although no attempt at quantification is made here. Finally, the laser pulses are not transform limited, with $\Delta\nu_{1/2}^L$ being much larger than the value estimated by one assuming the Fourier-transform limit to hold.⁷¹ Nevertheless, it is clear that in the present experiments the linear range extends to approximately 30 mW of pump power, and excited-state lifetimes were obtained by using pump powers below this value.

For pumping of the $3S_{1/2} \rightarrow 3P_{3/2}$ transition and probing of the $3P_{3/2} \rightarrow 4D_{5/2,3/2}$ transition, the ASOPS signal is described by Eq. (32). This expression reflects the above linear behavior with pump power W_{13} in the absence of saturation. Equation (32) predicts that if the ASOPS signal is divided by probe power

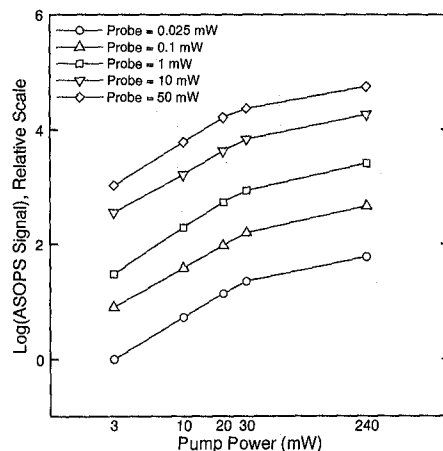


Fig. 11. ASOPS signal versus pump power for each probe power. Because of the large range of pump and probe powers, a log-log scale is used.

W_{34} , then the five lines of Fig. 11 should collapse to a single curve. If the experimental ASOPS signal is divided by probe power, the plot of Fig. 12 results. As shown, the individual lines do tend to converge, although the convergence is not perfect. This probably results from fluctuations of sodium concentration in the probe volume during the course of the experiments. Completion of the entire experiment required several hours, which allowed ample time for sodium concentration fluctuations to take place. If the deviation of curves in Fig. 12 is attributed entirely to variations in N_T , then the sodium population is estimated to fluctuate by approximately a factor of two.

The ASOPS signal is plotted versus probe power for each pump power on a log-log scale in Fig. 13. The linear behavior with probe power W_{34} is in good agreement with Eq. (32). Saturation is noticeably absent in each case. If the ASOPS signal of Eq. (32) is divided by the pump-beam power, the resulting equation predicts that the five plots of Fig. 13 should again collapse to a single curve. As shown in Fig. 14, the lines do indeed converge, although the convergence is again not perfect, owing to a factor of two for fluctuation in a sodium population.

In the stepwise excitation experiments of Omenetto *et al.*⁷² and Nitz *et al.*,⁷³ photoionization of the $4D$ level of atomic sodium was found to be significant. It is also possible that stepwise photoionization is significant during ASOPS measurements because of the excitation schemes that are used. The energy of the sodium $4D_{3/2,5/2}$ level is only 6892 cm^{-1} below that of the ionization threshold, and thus 568.8-nm probe photons could photoionize these atoms.⁷⁴ The stimulated photoionization-rate coefficient is given by¹¹

$$W_{\text{ION}} = \frac{\sigma_{\text{ION}} I}{h\nu_0}, \quad (39)$$

where σ_{ION} is the photoionization cross section (in squared centimeters) and ν_0 is the laser frequency (inverse seconds). For the $4D_{5/2}$ level, $\sigma_{\text{ION}} = 1.52 \times$

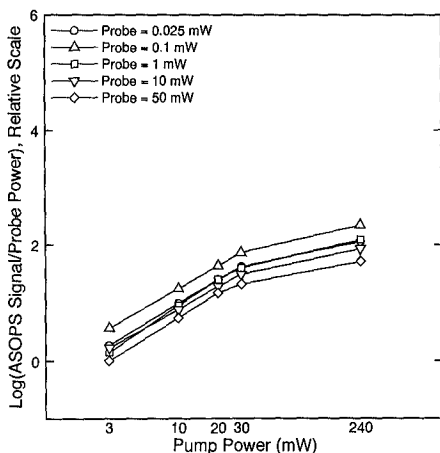


Fig. 12. ASOPS signal divided by probe power versus pump power (for each probe power). Because of the large range of pump and probe powers, a log-log scale is used.

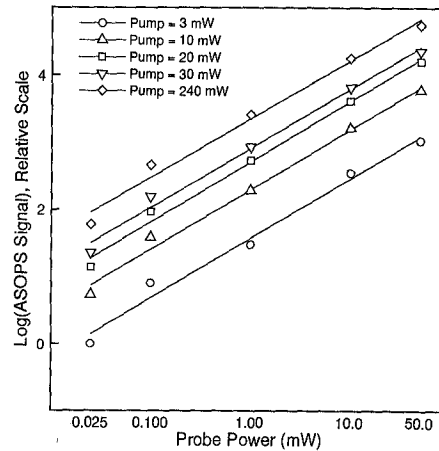


Fig. 13. ASOPS signal versus probe power (for each pump power). Because of the large range of pump and probe powers, a log-log scale is used.

10^{-17} cm^2 at the ionization threshold.⁷⁵ Assuming the cross section decreases with the cube of the laser frequency,⁷⁶ we find that a value of $1.97 \times 10^{-18} \text{ cm}^2$ results at 568.8 nm. Noting that the quantity hB_{12}/c is measured in units of squared centimeters, we see that the stimulated absorption-rate coefficient of Eq. (38) can be written in terms of the absorption cross section σ_{ABS} by the relation²⁸

$$W_{12} = \frac{2\sigma_{\text{ABS}} I}{\pi h \Delta\nu_{1/2} L}, \quad (40)$$

where $\sigma_{\text{ABS}} = 4.5 \times 10^{-18} \text{ cm}^2$ for the $3P_{3/2} \rightarrow 4D_{5/2}$ transition.⁶² Taking the ratio of the respective stimulated rate coefficients, the following expression enables a comparison of the relative magnitudes of photoionization and absorption:

$$\frac{W_{\text{ION}}}{W_{12}} = \left(\frac{\pi \Delta\nu_{1/2} L}{2\nu_0} \right) \left(\frac{\sigma_{\text{ION}}}{\sigma_{\text{ABS}}} \right). \quad (41)$$

For the $4D_{5/2}$ level, this ratio becomes 6.5×10^{-5} , and

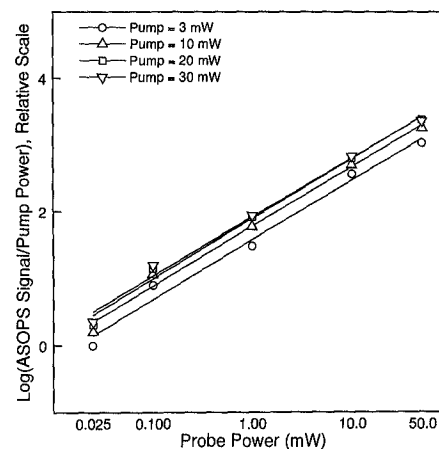


Fig. 14. ASOPS signal divided by pump power versus probe power (for each pump power). Because of the large range of pump and probe powers, a log-log scale is used.

hence photoionization is not important in ASOPS experiments with the probe laser at 568.8 nm. For the probe laser in resonance with the $3P_{1/2} \rightarrow 5S_{1/2}$ transition at 615.4 nm, a similar calculation results in a ratio of 1.2×10^{-7} , so that photoionization is even less likely.

Signals obtained in the initial application of ASOPS in a flame environment contained an unexplained negative artifact at the end of the free temporal range.⁴⁹ We now believe that perturbed free-induction decay^{77,78} may be the cause of this signal. An important assumption in the application of the rate equations is the absence of coherent transient effects. If the lifetime of the excited state is much larger than the temporal width of the incident light pulses, this assumption may not hold.^{2,68} Even when the assumption is violated, coherent effects may still be masked by averaging over the pulse-to-pulse intensity fluctuations of conventional pulsed lasers with free-running modes. Since mode-locked lasers define a fixed phase relationship among all active modes, they are ideal tools for observing coherent transients. In previous work,⁴⁹ both beams were tuned to the $3S_{1/2} \rightarrow 3P_{3/2}$ transition of sodium. Owing to the nature of the process, perturbed free-induction decay should not be observed when the pump beam remains tuned to the $3S_{1/2} \rightarrow 3P_{3/2}$ transition and the probe is tuned to the excited $3P_{3/2} \rightarrow 5S_{1/2}$ transition (Fig. 10). As expected, a negative signal is never observed in this configuration.⁶⁵

VI. Conclusions

A rate equation theory has been presented for ASOPS measurements. When the theory is used to analyze experimentally obtained sodium excited-state lifetimes, a $3P_{3/2} \rightarrow 3S_{1/2}$ decay time of 581 ps and a $3P_{3/2} \rightarrow 3P_{1/2}$ doublet-mixing time of 273 ps are obtained, in excellent agreement with published results. The predicted linear behavior of the ASOPS signal with pump and probe irradiance is then experimentally verified over several orders of magnitude of pump and probe beam power.

Experimental verification of the temporal ASOPS theory has been made possible by a significant improvement in the SNR over previous ASOPS measurements in flames.⁴⁹ In the initial experiments, a peak SNR of 33:1 resulted after 2056 averages. The average pump-beam power was ~ 3 times larger than that of the present study, but a 400-mm focal-length lens was used. The interaction length in the initial study was ~ 1 cm, compared with the present value of ~ 500 μm . In the initial study, the probe beam was tuned to the $3S_{1/2} \rightarrow 3P_{3/2}$ transition, which is characterized by a stimulated absorption-rate coefficient 48 times larger than that of the $3P_{1/2} \rightarrow 5S_{1/2}$ transition. For the current study, étalons in each dye-laser cavity reduce the laser bandwidth by approximately a factor of 3, but they also reduce peak power, so that this effect can be ignored. NaCl solutions were at least five times more concentrated in the earlier ASOPS studies. Considering these changes, we see that the cur-

rent SNR is certainly increased by several orders of magnitude compared to our previous results.

This improvement reflects favorably on the eventual detection of naturally occurring flame radicals. Our ultimate goal is to detect OH, since its resonances fall within the frequency-doubled output of the dye lasers. The expected reduction in the SNR will be significant, with a reduction in the Einstein rate coefficient from that of sodium by three orders of magnitude. Moreover, a sizeable drop in available laser power and beam quality will result, owing to the inefficiency of frequency doubling for the mode-locked laser systems, although nearly 30 mW of second-harmonic output has recently been obtained in our laboratory.⁷⁹ Experiments demonstrated in this paper show that the present ASOPS detection scheme falls far short of the shot-noise limit. Moreover, frequency doubling will significantly increase the baseband noise.⁵³ Indeed, initial attempts at obtaining OH lifetimes by using the ASOPS method have not been successful.⁸⁰ Recent improvements in mode-locked laser technology have been shown to significantly improve laser operation.⁸¹⁻⁸³ Several of these advances are presently being implemented. A particularly intriguing development is the optical feedback technique, which has recently been demonstrated to substantially reduce dye-laser noise and result in transform-limited pulses.^{71,84} We are presently evaluating the technique for use on the pump and the probe dye lasers.

It is also possible to relocate the beat frequency in order to enhance the SNR. Fig. 5 suggests that a beat frequency of above 400 kHz would reduce noise by over 30 dB from the present case. A frequency analysis of the ASOPS signal of Fig. 10 predicts that it may be necessary to retain ~ 100 harmonics to prevent excessive distortion.⁶⁵ Moreover, the Nyquist sampling theorem requires that the signal bandwidth must be kept below 41 MHz for the present mode-locking frequencies. Thus the optimum beat frequency is probably located somewhat below 400 kHz. Even at this increased frequency, a single scan time of 2.5 μsec results, and since signal averaging would likely remain necessary, the turbulence spectral information would in turn be limited to the millisecond regime. Although such information would be a valuable tool, the beat frequency could be extended by using third-harmonic mode locking of the Nd:YAG laser systems. The resulting 246-MHz mode-locking frequency would allow a beat frequency of over 1 MHz.⁴⁸ Since the present ASOPS results are obtained in a time scale that falls far short of the regime required for turbulent combustors, it will clearly be necessary to change the pump, probe, and beat frequencies in this manner.

The differential detection circuit described in this paper, even though it reduces noise by ~ 20 dBm, is difficult to use since the reference and signal beam irradiances must be carefully matched. A remarkable noise cancellation circuit has recently been shown by Hobbs to reduce baseband noise by over 50 dBm^{85,86}

and it does not require the reference and signal irradiances to be carefully balanced. This circuit is presently being added to our instrument.

This research was sponsored by the U. S. Air Force Office of Scientific Research, Air Force Systems Command, under grant AFOSR-84-0323. G. J. Fiechtner gratefully acknowledges the support of a Shell Companies Foundation Doctoral Fellowship. The authors thank R. J. Kneisler, Department of Chemistry, Purdue University, for maintenance of the mode-locked Nd:YAG lasers for and his helpful suggestions concerning these experiments and C. D. Carter, Flame Diagnostics Laboratory, Purdue University, for use of the flat-flame burner.

References

1. A. C. Eckbreth, *Laser Diagnostics for Combustion Temperature and Species* (Abacus, Cambridge, Mass., 1988).
2. R. P. Lucht, "Applications of laser-induced fluorescence spectroscopy for combustion and plasma diagnostics," in *Laser Spectroscopy and Its Applications*, L. J. Radziemski, R. W. Solarz, and J. A. Paisner, eds. (Dekker, New York, 1987), pp. 623-673.
3. C. D. Carter, G. B. King, and N. M. Laurendeau, "A combustion facility for high-pressure flame studies by spectroscopic methods," *Rev. Sci. Instrum.* **60**, 2606-2609 (1989).
4. C. D. Carter, "Saturated fluorescence measurements of the hydroxyl radical in laminar high-pressure flames," Ph.D. dissertation (Purdue University, West Lafayette, Ind., 1990).
5. R. Suntz, H. Becker, P. Monkhouse, and J. Wolfrum, "Two-dimensional visualization of the flame front in an internal combustion engine by laser-induced fluorescence of OH radicals," *Appl. Phys.* **47B**, 287-293 (1988).
6. K. Kohse-Höinghaus, U. Meier, and B. Attal-Trétout, "Laser-induced fluorescence study of OH in flat flames of 1-10 bar compared with resonance CARS experiments," *Appl. Opt.* **29**, 1560-1569 (1990).
7. J. W. Daily, "Pulsed resonance spectroscopy applied to turbulent combustion flows," *Appl. Opt.* **15**, 955-960 (1976).
8. R. P. Lucht, D. W. Sweeney, and N. M. Laurendeau, "Time-resolved fluorescence investigation of rotational transfer in $A^2\Sigma^+$ ($v = 0$) OH," *Appl. Opt.* **25**, 4086-4095 (1986).
9. C. D. Carter, J. T. Salmon, G. B. King, and N. M. Laurendeau, "Feasibility of hydroxyl measurements by laser-saturated fluorescence in high-pressure flames," *Appl. Opt.* **26**, 4551-4562 (1987).
10. J. T. Salmon and N. M. Laurendeau, "Calibration of laser-saturated fluorescence measurements using Rayleigh scattering," *Appl. Opt.* **24**, 65-72 (1985).
11. J. T. Salmon and N. M. Laurendeau, "Absolute concentration measurements of atomic hydrogen in subatmospheric pre-mixed $H_2/O_2/N_2$ flat flames with photoionization controlled-loss spectroscopy," *Appl. Opt.* **26**, 2881-2891 (1987).
12. P. Andresen, A. Bath, W. Gröger, H. W. Lulf, G. Meijer, and J. J. ter Meulen, "Laser-induced fluorescence with tunable excimer lasers as a possible method for instantaneous temperature field measurements at high pressures: checks with an atmospheric flame," *Appl. Opt.* **27**, 365-378 (1988).
13. R. S. Barlow, R. W. Dibble, and R. P. Lucht, "Simultaneous measurement of Raman scattering and laser-induced OH fluorescence in nonpremixed turbulent jet flames," *Opt. Lett.* **14**, 263-265 (1989).
14. R. S. Barlow, R. W. Dibble, J.-Y. Chen, and R. P. Lucht, "Effect of Damkohler number on superequilibrium OH concentration in turbulent nonpremixed jet flames," *Rep. AIAA-89-0061* (American Institute of Aeronautics and Astronautics, Washington, D.C., 1989).
15. K. J. Rensberger, M. J. Dyer, and R. A. Copeland, "Time-resolved CH ($A^2\Delta$ and $B^2\Sigma^-$) laser-induced fluorescence in low-pressure hydrocarbon flames," *Appl. Opt.* **27**, 3679-3689 (1988).
16. R. J. Cattolica, J. A. Cavalowsky, and T. G. Mataga, "Laser-induced fluorescence measurements of nitric oxide in low-pressure $H_2/O_2/NO$ flames," in *Twenty-Second Symposium (International) on Combustion* (The Combustion Institute, Pittsburgh, Pa., 1988), pp. 1165-1173.
17. Y. Takubo, T. Okamoto, N. Komine, and M. Yamamoto, "Absolute density measurement of OH radicals in an atmospheric pressure flame using time-resolved laser-induced fluorescence," *Jpn. J. Appl. Phys.* **26**, 416-418 (1987).
18. M. J. Wirth, "Ultrafast spectroscopy," *Anal. Chem.* **62**, 270A-277A (1990).
19. N. S. Bergano, P. A. Jaanimagi, M. M. Salour, and J. H. Bechtel, "Picosecond laser-spectroscopy measurement of hydroxyl fluorescence lifetimes in flames," *Opt. Lett.* **8**, 443-445 (1983).
20. R. Schwarzwald, P. Monkhouse, and J. Wolfrum, "Picosecond fluorescence lifetime measurement of the OH radical in an atmospheric pressure flame," *Chem. Phys. Lett.* **142**, 15-18 (1987).
21. R. Schwarzwald, P. Monkhouse, and J. Wolfrum, "Fluorescence studies of OH and CN radicals in atmospheric pressure flames using picosecond excitation," in *Twenty-Second Symposium (International) on Combustion* (Combustion Institute, Pittsburgh, Pa., 1988), pp. 1413-1420.
22. R. Schwarzwald, P. Monkhouse, and J. Wolfrum, "Fluorescence lifetimes for nitric oxide in atmospheric pressure flames using picosecond excitation," *Chem. Phys. Lett.* **158**, 60-64 (1989).
23. H. Tennekes and J. L. Lumley, *A First Course in Turbulence* (MIT, Cambridge, Mass., 1981), pp. 19-20, 67-68.
24. T. S. Cheng, J. A. Wehrmeyer, R. W. Pitz, O. Jarret, Jr., and G. B. Northam, "Finite-rate chemistry effects in a Mach 2 reacting flow," *Rep. AIAA-91-2320* (American Institute of Aeronautics and Astronautics, Washington, D.C., 1991).
25. R. Goulard, A. M. Mellor, and R. W. Bilger, "Combustion measurements in air-breathing propulsion engines. Survey and research needs," *Combust. Sci. Technol.* **14**, 195-219 (1976).
26. A. J. Alfano, "Approach for a quantitative on-the-fly fluorescence diagnostic in combustion systems," *Appl. Opt.* **28**, 5010-5015 (1989).
27. A. J. Alfano, F. K. Fong, and F. E. Lytle, "High repetition rate subnanosecond gated photon counting," *Rev. Sci. Instrum.* **54**, 967-972 (1983).
28. F. E. Lytle, "Laser fundamentals," in *Lasers in Chemical Analysis*, G. M. Hieftje, J. C. Travis, and F. E. Lytle, eds. (Humana, Clifton, N.J., 1981), pp. 3-39.
29. G. Kychakoff, R. D. Howe, and R. K. Hanson, "Spatially resolved combustion measurements using cross-beam saturated absorption spectroscopy," *Appl. Opt.* **23**, 1303-1306 (1984).
30. J. E. M. Goldsmith, "Spatially resolved saturated absorption spectroscopy in flames," *Opt. Lett.* **6**, 525-527 (1981).
31. R. L. Farrow and L. A. Rahn, "Spatially resolved infrared absorption measurements: application of an optical Stark effect," *Opt. Lett.* **6**, 108-110 (1981).
32. J. E. M. Goldsmith and R. L. Farrow, "Spatially resolved optical Stark-modulation spectroscopy in flames," *Opt. Lett.* **7**, 215-217 (1982).
33. P. E. Walters, J. Lanauze, and J. D. Winefordner, "Spatially resolved concentration studies of ground state atoms in a

- flame: saturated absorption spectroscopic method," *Spectrochim. Acta* **42B**, 125–129 (1984).
34. N. Omenetto, G. C. Turk, M. Rutledge, and J. D. Winefordner, "Atomic and ionic fluorescence dip spectroscopy as a tool for flame and plasma diagnostics," *Spectrochim. Acta* **42B**, 807–817 (1987).
 35. T. Edwards, D. P. Weaver, and D. H. Campbell, "Laser-induced fluorescence in high-pressure solid-propellant flames," *Appl. Opt.* **26**, 3496–3509 (1987).
 36. G. J. Blanchard and M. J. Wirth, "Measurement of small absorbances by picosecond pump-probe spectrometry," *Anal. Chem.* **58**, 532–535 (1986).
 37. M. J. Wirth and G. J. Blanchard, "Picosecond spectroscopy in analytical chemistry," in *Analytical Applications of Lasers*, E. H. Piepmeier, ed. (Wiley, New York, 1986), pp. 477–492.
 38. J. P. Heritage and D. L. Allara, "Surface picosecond Raman gain spectra of a molecular monolayer," *Chem. Phys. Lett.* **74**, 507–510 (1980).
 39. B. F. Levine and C. G. Bethea, "Ultrahigh sensitivity stimulated Raman gain spectroscopy," *IEEE J. Quantum Electron.* **QE-16**, 85–89 (1980).
 40. J. Baran, D. Elliot, A. Grofcsik, W. J. Jones, M. Kubinyi, A. J. Langley, and V. U. Nayar, "Raman amplification spectroscopy using mode-locked lasers," *J. Chem. Soc. Faraday Trans. 2* **79**, 865–883 (1983).
 41. J. P. Heritage, "Picosecond nonlinear spectroscopy of silver microstructures and surface adsorbates," in *Advances in Laser Spectroscopy 2*, B. A. Garetz and J. R. Lombardi, eds. (Wiley, New York, 1983), pp. 207–224.
 42. A. J. Langley, R. A. Beaman, J. Baran, A. N. Davies, and W. J. Jones, "Concentration-modulated absorption spectroscopy," *Opt. Lett.* **10**, 327–329 (1985).
 43. A. J. Langley, R. A. Beaman, A. N. Davies, W. J. Jones, and J. Baran, "Concentration-modulated absorption spectroscopy I," *Chem. Phys.* **101**, 117–125 (1986).
 44. R. A. Beaman, A. N. Davies, A. J. Langley, W. J. Jones, and J. Baran, "Concentration-modulated absorption spectroscopy II. Temporal variation of gain," *Chem. Phys.* **101**, 127–132 (1986).
 45. G. R. Fleming, *Chemical Applications of Ultrafast Spectroscopy* (Oxford U. Press, New York, 1986).
 46. P. A. Elzinga, F. E. Lytle, Y. Jiang, G. B. King, and N. M. Laurendeau, "Pump/probe spectroscopy by asynchronous optical sampling," *Appl. Spectrosc.* **41**, 2–4 (1987).
 47. P. A. Elzinga, R. J. Kneisler, F. E. Lytle, Y. Jiang, G. B. King, and N. M. Laurendeau, "A pump/probe method for fast analysis of visible spectral signatures utilizing asynchronous optical sampling," *Appl. Opt.* **26**, 4303–4309 (1987).
 48. R. J. Kneisler, F. E. Lytle, G. J. Fiechtner, Y. Jiang, G. B. King, and N. M. Laurendeau, "Asynchronous optical sampling: a new combustion diagnostic for potential use in turbulent, high-pressure flames," *Opt. Lett.* **14**, 260–262 (1989).
 49. G. J. Fiechtner, Y. Jiang, G. B. King, N. M. Laurendeau, R. J. Kneisler, and F. E. Lytle, "Determination of relative number density and decay rate for atomic sodium in an atmospheric premixed flame by asynchronous optical sampling," in *Twenty-Second Symposium (International) on Combustion* (Combustion Institute, Pittsburgh, Pa., 1988), pp. 1915–1921.
 50. D. Stepowski and M. J. Cottreau, "Direct measurement of OH local concentration in a flame from the fluorescence induced by a single laser pulse," *Appl. Opt.* **18**, 354–356 (1979).
 51. D. Stepowski and M. J. Cottreau, "Study of the collisional lifetime of hydroxyl (${}^2\Sigma^+$, $v' = 0$) radicals in flames by time-solved laser-induced fluorescence," *Combust. Flame* **40**, 65–70 (1981).
 52. R. J. Cattolica, D. Stepowski, D. Puechberty, and M. Cottreau, "Laser-induced fluorescence of the CH molecule in a low-pressure flame," *J. Quant. Spectrosc. Radiat. Transfer* **32**, 363–370 (1984).
 53. D. Von der Linde, "Characterization of the noise in continuously operating mode-locked lasers," *Appl. Phys. B* **39**, 201–217 (1986).
 54. A. H. Lefebvre, *Gas Turbine Combustion* (Hemisphere, New York, 1983).
 55. A. J. Hynes, M. Steinberg, and K. Schofield, "The chemical kinetics and thermodynamics of sodium species in oxygen-rich hydrogen flames," *J. Chem. Phys.* **80**, 2585–2597 (1984).
 56. G. Herzberg, *Atomic Spectra and Atomic Structure* (Dover, New York, 1984).
 57. C. Th. J. Alkemade, "Anomalous saturation curves in laser-induced fluorescence," *Spectrochim. Acta* **40B**, 1331–1368 (1985).
 58. R. P. Lucht and N. M. Laurendeau, "Comment on 'Laser-induced fluorescence measurement of sodium in flames,'" *Combust. Flame* **34**, 215–217 (1979).
 59. Y. Takubo, T. Okamoto, and M. Yamamoto, "Laser spectroscopic measurement of quenching and doublet mixing rates of the Na ($3P_{3/2,1/2}$) doublet in a propane-air flame," *Appl. Opt.* **25**, 740–743 (1986).
 60. R. E. Russo and G. M. Hieftje, "Determination of atomic and molecular excited-state lifetimes using an optoelectronic cross-correlation method," *Appl. Spectrosc.* **36**, 92–99 (1982).
 61. J. T. Fourkas, T. R. Brewer, H. Kim, and M. D. Fayer, "Picosecond time-resolved four-wave mixing experiments in sodium-seeded flames," *Opt. Lett.* **16**, 177–179 (1991).
 62. W. L. Wiese and G. A. Martin, "Atomic transition probabilities," in *CRC Handbook of Chemistry and Physics*, R. C. Weast and M. A. Astle, eds. (CRC, Boca Raton, Fla., 1982).
 63. Y. Takubo, T. Okamoto, M. Yamamoto, "Laser spectroscopic measurement of subnanosecond fluorescence lifetime of Na $3P$ level in atmospheric N_2 gas," *Jpn. J. Appl. Phys.* **24**, L263–L265 (1985).
 64. W. Demtroder, *Laser Spectroscopy* (Springer-Verlag, New York, 1981).
 65. G. J. Fiechtner, "Measurements of atomic sodium in flames by asynchronous optical sampling," M. S. thesis (Purdue University, West Lafayette, Ind., 1989).
 66. C. Th. J. Alkemade, Tj. Hollander, W. Snelleman, and P. J. Th. Zeegers, *Metal Vapours in Flames* (Pergamon, New York, 1982).
 67. G. Zizak, "Laser diagnostics in flames by fluorescence techniques," in *Analytical Laser Spectroscopy*, S. Martellucci and A. N. Chester, eds. (Plenum, New York, 1985), pp. 147–157. The ratio in this case is actually given as $(Q + A)/Q_{32}$.
 68. R. Altkorn and R. N. Zare, "Effects of saturation on laser-induced fluorescence measurements of population and polarization," *Ann. Rev. Phys. Chem.* **35**, 265–289 (1984).
 69. J. T. Salmon and N. M. Laurendeau, "Analysis of probe volume effects associated with laser-saturated fluorescence measurements," *Appl. Opt.* **24**, 1313–1321 (1985).
 70. W. Mallawaarachchi, A. N. Davies, R. A. Beaman, A. J. Langley, and W. J. Jones, "Concentration-modulated absorption spectroscopy. Part 4—The use of continuous-wave lasers," *J. Chem. Soc. Faraday Trans. 2* **83**, 707 (1987).
 71. C. J. Hooker, J. M. D. Lister, and I. N. Ross, "Variable length transform-limited pulses from a stabilized synchronously-pumped mode-locked laser," *Opt. Commun.* **80**, 375–380 (1991).
 72. N. Omenetto, M. Leong, C. Stevenson, J. Vera, B. W. Smith, and J. D. Winefordner, "Fluorescence dip spectroscopy of sodium atoms in an inductively coupled plasma," *Spectrochim. Acta* **43B**, 1093–1100 (1988).
 73. D. E. Nitz, A. V. Smith, M. D. Levenson, and S. J. Smith,

- “Bandwidth-induced reversal of asymmetry in optical-optical-resonance amplitudes,” *Phys. Rev. A* **24**, 288–293 (1981).
74. O. Axner, “Determination of optimum conditions for laser-enhanced ionization spectrometry in flames—I. One-step signal strength versus excitation transition,” *Spectrochim. Acta* **45B**, 561–579 (1990).
 75. A. V. Smith, J. E. M. Goldsmith, D. E. Nitz, and S. J. Smith, “Absolute photoionization cross-section measurements of the excited 4D and 5S states of sodium,” *Phys. Rev. A* **22**, 577–581 (1980).
 76. D. E. Rothe, “Radiative ion-electron recombination in a sodium-seeded plasma,” *J. Quant. Spectrosc. Radiat. Transfer* **9**, 49–62 (1969).
 77. C. H. Brito Cruz, J. P. Gordan, P. C. Becker, R. L. Fork, and C. V. Shank, “Dynamics of spectral hole burning,” *IEEE J. Quantum Electron.* **QE-24**, 261–264 (1988).
 78. M. Joffre, D. Hulin, A. Migus, A. Antonetti, C. Benoit a la Guillaume, N. Peyghambarian, M. Lindberg, and S. W. Koch, “Coherent effects in pump-probe spectroscopy of excitons,” *Opt. Lett.* **13**, 276–278 (1988).
 79. G. J. Fiechtner, G. B. King, N. M. Laurendeau, R. J. Kneisler, and F. E. Lytle, “Efficient frequency doubling for synchronously mode-locked dye lasers,” *Appl. Spectrosc.* **43**, 1286–1287 (1989).
 80. R. J. Kneisler, “Construction and development of a picosecond UV pump/UV probe spectrometer for combustion diagnostics based on asynchronous optical sampling (ASOPS),” Ph.D. dissertation (Purdue University, West Lafayette, Ind., 1990).
 81. H. Vanherzeele, “Characterization and active stabilization of a harmonically modulated continuous-wave Nd:LiYF₄ laser,” *Rev. Sci. Instrum.* **60**, 592–597 (1989).
 82. M. J. W. Rodwell, D. M. Bloom, and K. J. Weingarten, “Subpicosecond laser timing stabilization,” *IEEE J. Quantum Electron.* **25**, 817–827 (1989).
 83. K. Ibbs, “Ultrafast laser systems—comparing technologies,” *Lasers Optron.* **9**(2), 39–50 (1990).
 84. D. S. Peter, P. Beaud, W. Hodel, and H. P. Weber, “Passive stabilization of a synchronously pumped mode-locked dye laser with the use of a modified output coupling mirror,” *Opt. Lett.* **16**, 405–407 (1991).
 85. P. C. D. Hobbs, “Reaching the shot noise limit for \$10,” *Opt. Photon. News* **1**(4), 17–23 (1991).